Multi-parameter Improvement Method for (Micro-) Structural Properties of High Performance Ceramics

G Boiger[1]*, T Ott[1], L Holzer[1], D Penner[2], M Gorbar[2],Y Hasan[2]

1. ICP Institute of Computational Physics, School of Engineering, Zurich University of Applied Sciences, Winterthur, Switzerland

2. IMPE Institute of Materials and Process Engineering, School of Engineering, Zurich University of Applied Sciences, Winterthur, Switzerland

ABSTRACT

Many pH-measurement electrodes rely on porous diaphragms to create a liquid electrolyte junction between reference-electrolyte and the fluid to be measured. In field applications, the diaphragm is required to meet partly contradictory improvement criteria. To minimize measurement errors and to ensure durability of the measurement device, the diaphragm is supposed to maximize electrolyte conductivity and reference-electrolyte outflow velocity, while simultaneously minimizing reference electrolyte flow rate. The task of optimizing the overall performance of this small piece of ceramics has lead to the development of a novel multi-parameter improvement scheme for its (micro-) structural design. The method encompasses the consideration of microscopic material design parameters, such as porosity, pore- tortuosity and constrictivity, macroscopic material parameters such as diaphragm diameter and length, as well as process parameters like internal electrode pressure or the electrolyte viscosity and specific resistivity. Comprising sets of design parameters to dimensionless groups, concrete design guidelines as well as the introduction of a three-dimensional improvement space concept are proposed. The novel design space concept allows the improvement of each possible diaphragm-based measurement set-up, by considering the simultaneous, dimensionless interaction of all relevant design parameters.

1. INTRODUCTION

Many pH-probes require a liquid junction between a reference electrolyte and the substrate solution. Its main task is to provide a conductive bridge between the two liquids, while simultaneously preventing the reference electrolyte to be polluted by substrate ions [4]. In the case of this study, the device in charge of maintaining such a junction is a small, cylindrical, porous piece of ceramics, D_{dia}= 1 mm in width, L_{dia}= 2 mm in length, referred to as diaphragm [5]-[7]. A schematic illustration of the type of pH-probes in question is shown in Figure 1 [1].

*Corresponding Author: gernot.boiger@zhaw.ch

The overall task within this research is to conduct knowledge-based improvement of existing macro- and micro-structural diaphragm design options. Thereby diaphragm-improvement shall be defined as an increase of probe durability and a simultaneous decrease of measurement errors, which co-occur with too little junction-conductivity or ionic pollution of the reference electrolyte [8], [9].

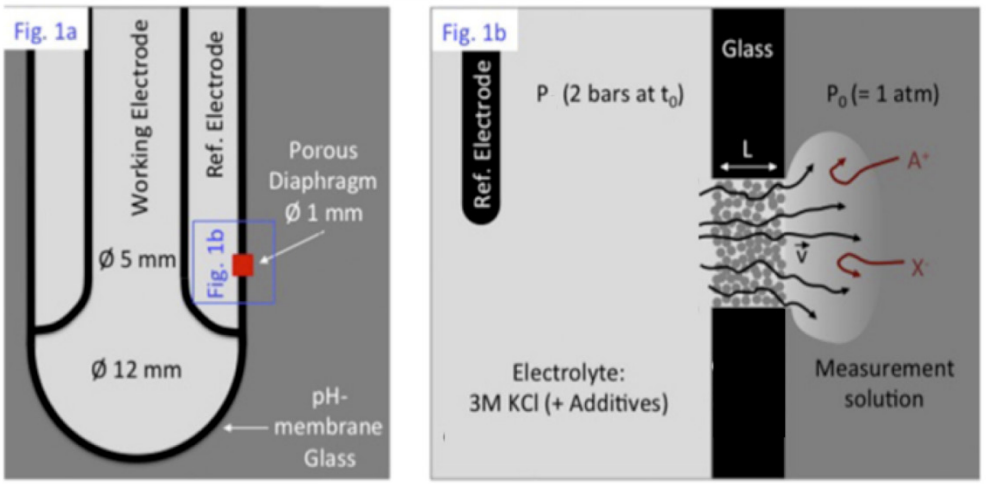

Figure 1: Schematic illustration of the pH-probe (1a) and of the liquid junction (diaphragm) inside the probe [1].

1.1. Functionality of Porous Diaphragms

The pH-measurement set-up under consideration, features a pressurized ($p \approx 2.0$bar) reference electrolyte (3M KCl + additives), which is contained within a reference glass electrode, as seen in Figure 1, left [1], [10]. The diaphragm both separates and connects the internal reference electrolyte and the external measurement solution. On the one hand the diaphragm's pores constitute a passage for electrons [e-], thus providing the necessary conductivity S_{ohm} for the measurement procedure. On the other hand, anions [A+] or cations [X-], dissolved in the external measurement solution tend to diffuse through the pores to the inside and thus pollute the reference electrolyte [5]-[7|. While the first effect is strongly desired, the latter is to be averted as well as possible, since measurement accuracy decreases with increasing electrolyte pollution. Thus a flux of reference electrolyte, induced by the pressure gradient over the length of the diaphragm, is used to flush out substrate-ions diffusing upstream. This means that gradual reference electrolyte is accepted for the sake of measurement accuracy [10].

The bottom line at this point is, that the "ideal" porous diaphragm has to fulfill several, partly contradicting tasks:

(i) Provide much open cross sectional area A_{dia}, in order to achieve highest possible conductivity S_{ohm}.

(ii) Flush out most external ions by inducing highest possible maximum outflow velocities vmax within the pores.

(iii) Ensure maximum probe durability, namely minimum electrolyte depletion, by minimizing electrolyte outflow rate $\dot{V}$.

1.2. Characterization of Diaphragm Microstructure

Obviously, the task of improving diaphragm functionality, as described in chapter 1.1, goes beyond the adaption of macrostructure parameters, such as diaphragm length L_{dia} or width D_{dia}. It has to entail a thorough study and controlled adaption of related microstructure parameters in relation to porosity, pore- shapes and sizes.

As proposed in [1] and [11]-[21], three main micro-structural parameters are chosen to characterize a diaphragm's pore collective: (i) diaphragm porosity, (ii) pore constrictivity and (iii) pore tortuosity. They shall shortly be described in the following.

1.2.1. Diaphragm Porosity ε_{dia}(-)

The dimensionless porosity of the diaphragm, defined in Equ.1 and sketched in Figure 2 (top section), relates the total pore volume V_p to the total volume of the diaphragm V_{dia}.

$$\varepsilon_{dia} = \frac{V_p}{V_{dia}} \tag{1}$$

A sensible variation of this quantity is the open pore porosity $\varepsilon_{dia,eff}$, which is defined by Equ.2 and only considers open pore space, effectively filled with electrolyte $V_{p,eff}$.

$$\varepsilon_{dia,eff} = \frac{V_{p,eff}}{V_{dia}} \tag{2}$$

1.2.2. Pore Constrictivity β_p(-)

The dimensionless constrictivity, defined by Equ.3 and sketched in Figure 2 (middle section), is a measure for the occurrence of pore-bottlenecks and relates minimum pore diameters $D_{p,min}$ to maximum pore diameters $D_{p,max}$.

$$\beta_p = \left(\frac{D_{p,\min}}{D_{p,\max}} \right)^2 \tag{3}$$

According to this definition, a high constrictivity (β_p->1) means that the majority of all pores have constant diameters, while a low constrictivity (β_p->0) means that most pores feature extremely defined, very narrow bottlenecks, [17], [18].

1.2.3. Pore Tortuosity τ_p(-)

The dimensionless pore tortuosity, shown in Equ.3 and sketched in Figure 2 (bottom section), is the ratio between the effective pore length Lp and the minimum possible pore length, which is the actual diaphragm length L_{dia}.

$$\tau_p = \frac{L_p}{L_{dia}} \tag{4}$$

While a low tortuosity (τ_p->1) means that the majority of all pores are almost straight, a high tortuosity (τ_p>>1) means that the ceramic structure features many highly twisted pores,[11], [13], [14] and [18].

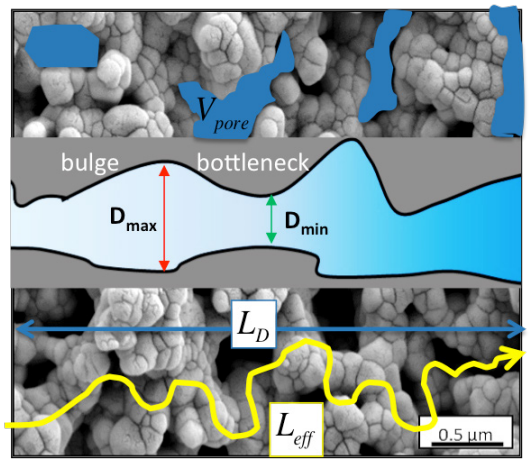

Figure 2: Sketch of the micro-structural parameters porosity (top section), constrictivity (middle section) and tortuosity (bottom section). [1], [2].

1.3. How to adapt Structural Parameters

Microstructure related parameters can be modified by adjusting production related parameters [2], [3]. One such example is shown in Figure 3. There porosity, tortuosity and constrictivity of three diaphragm prototypes, made out of one and the same material matrix, are varied due to gradual increase of the sintering temperature.

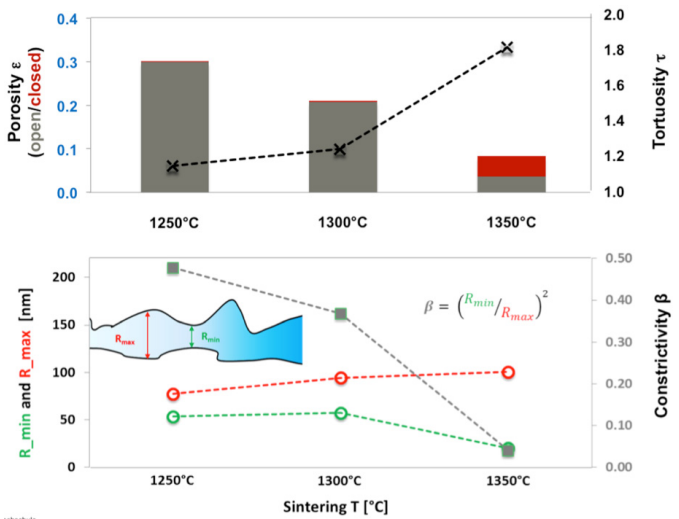

Figure 3: Total- and open porosity (top, grey + red beams combined and grey beams respectively), tortuosity (top, dashed grey line), constrictivity (bottom, dashed grey line), maximum pore radius R_{max} (bottom, dashed red line) and minimum pore radius R_{min} (bottom, dashed green line) against sintering temperature [1], [2] and [3].

2. THE MULTI-PARAMETER IMPROVEMENT METHOD

A method has been devised which accomplishes the following tasks:

(i) Definition of three distinct improvement criteria (chapter 2.1.2);

(ii) Derivation of a validated semi-analytical model, which relates the improvement criteria to all available degrees of freedom a.k.a. design parameters (chapters 2.1.1, 2.2.1 and 2.2.2);

(iii) Transfer to a dimensionless problem by the introduction of dimensionless design factors (chapter 2.2.3);

(iv) Derivation of measures to modify individual improvement criteria (chapter 2.2.4);

(v) Depiction of all occurring criteria-parameter-dependencies (see chapter 2.2.5);

(vi) Introduction of switching factors, which link the design parameters such that the shifting of focus from one improvement criterion to another can be conducted in a controlled fashion (chapter 2.2.6).

(vii) Evaluation and comparison of design options by introduction of the overall performance factor Ω.

2.1. Problem Definition

Since the given tasks in regard to diaphragm functionality involve flow-, conductivity-, process- and microstructure- related aspects, a thorough problem definition is necessary. This relates to laying out a clear picture of all possible degrees of freedom as well as an unmistakable statement regarding the aspects we wish to improve.

2.1.1. Design Parameters / Degrees of Freedom

Table 1 gives an overview of all degrees of freedom (=design parameters), their respective symbols, units and related, dimensionless design factors. The design parameters concern mainly ceramic macro- or microstructure, but also relate to the measurement process and electrolyte properties.

Table 1: Overview of design parameters and dimensionless design factors. *For definition of p, see chapter 2.2.1.

Parameter Type	**Design Parameter**	**Design Parameter Symbol Ψ_i**	**Unit of Ψ_i**	**Design Factor $F_{i,j}=\Psi_{i,j}+1/\Psi_{i,j}$ (-)**
Ceramic Macro-Structure	Length of Diaphragm	L_D	m	b
	Cross Section of Diaphragm	A_D	m^2	a
Ceramic Micro-Structure	Pore Constrictivity	β	-	f
	Pore Tortuosity	τ	-	g
	Porosity*	p_ε	-	e
Process	Pressure Difference	Δp	Pa	c
Electrolyte	Dynamic Viscosity	μ	Pas	d
	Intrinsic Resistivity	ρ_{ohm}	Ωm	h

2.1.2. Improvement Criteria

Based on the main objectives to increase sensor durability while simultaneously decreasing its measurement error rate, three distinct improvement criteria can be defined: the velocity criterion, the flow-rate criterion and the conductivity criterion.

Velocity Criterion

The velocity criterion, according Eqn.5, states that the maximum occurring outflow velocity vmax within the diaphragm's pores must be maximized in order to flush out as many diffusing ions as possible. The overall rate of ions diffusing upstream does not necessarily relate to average outflow velocities, but rather to the maximum encountered outflow velocity. The latter is likely to occur at bottleneck formations along the pores.

$$v_{\max} \rightarrow \max. \tag{5}$$

Flow-rate Criterion

The flow-rate criterion, according Eqn.6, states that the outgoing flow-rate of reference $\dot{V}$ electrolyte must be minimized in order to increase sensor lifetime. Obviously this criterion is contradictory to the velocity criterion, when applied to a given pore geometry.

$$\dot{V} \rightarrow \min. \tag{6}$$

Conductivity Criterion

The conductivity criterion, according Eqn.7, states that the electric conductivity S_{ohm} of the entire diaphragm must be maximized in order to let electrons pass as easily as possible, leading to a minimization of measurement errors at varying PH levels. Since e.g. wider, shorter pores will yield higher conductivity, this criterion, at first inspection, stands in contradiction to the flow-rate criterion but goes in-line with the velocity criterion.

$$S_{ohm} \rightarrow \max. \tag{7}$$

2.2. Semi-Analytical Model of Simplified Physics

A simplified, semi-analytical model has been created to derive generalized design-guidelines for material- and process parameters. The model has been validated by CFD calculations and is used to depict the full path from *improvement criteria* towards possible design options.

2.2.1. Connecting Improvement Criteria with Design Parameters

The basic model equations are shown in Table 2 and provide the context between *design parameters and improvement criteria*.

The model encompasses:

(i) A standard formulation for creeping pipe flow [23], [24] extended by the calculation of maximum outflow velocities at the bottlenecks and thus a relation to pore constrictivity β.

(ii) A formulation of the material's overall permeability K(m^2), according Eqn.8, [1] and [22], which relates microstructure aspects to this macrostructure property.

$$K = K_0 * w * M \tag{8}$$

In Eqn.8, K_0(m2) is the intrinsic permeability in relation to the ceramic surface

roughness, w(-) is a dimensionless proportionality constant (hereby chosen to be equal to 1 and thus unused) and M (-) is the dimensionless M-factor, or permeability factor, according Eqn.9. The latter includes the link to microstructure properties of the material.

$$M = \frac{(p*\varepsilon)^x * \beta^y}{\tau^{z+1}} \tag{9}$$

Based on [1], [12] and [17], the coefficients x, y and z in Eqn.9 are chosen as: 1.15, 0.37 and 4.39 respectively. In Eqn.9, p (m^3_{Dia}/m_p) is a proportionality factor which relates the porosity to the cross sectional area of an average pore. Thus p is defined by $p= n^{-1}*L_{Dia}*p'$, where n ($1/m^2_{Dia}$) is the number of pores per cross-sectional area of the diaphragm and p'(m^2_p/m^3_p) is a coefficient related to the porosity's isotropy, which is hereby assumed as 1.

(iii) Ohm's law of electric conductivity through electrolyte-filled pores.

(iv) The assumption that overall electric conductivity and permeability behave in 1:1 analogy to intrinsic material properties and the microstructure, [11], [12] and [21]. Thus it can be concluded that the overall electric conductivity of the electrolyte-filled diaphragm depends on the intrinsic electrolyte resistivity ρ_{ohm} (Ωm) and on the microstructure-related M-factor (Eqn.9).

(v) A formulation for the overall diaphragm-performance, or performance factor P, which shall be defined as an assembly of all process variables to be improved Φ_i and their respective improvement coefficients γ_i, according Eqn.10. Thereby γ_i is +1 in case of desired maximization and γ_i is -1 in case of desired minimization of the process variable.

$$P = \prod_i \phi_i^{\nu_i} = \frac{S_{ohm} * v_{\max}}{\dot{V}} \tag{10}$$

Table 2: Overview of process variables to be improved and their context to the design parameters according to the semi-analytic model.

Process Variable to be improved	**Quantity/Symbol Φ_i**	**Context to Design Parameters $\Phi_i = f(\Psi_i)$**
Maximum Outflow Velocity	$v_{\max}$	$\frac{1}{4}*\left[\frac{1}{\beta}+2*\frac{1}{\sqrt{\beta}}+1\right]*K_0*w*\frac{(p*\varepsilon)^x*\beta^y}{\tau^{z+1}}*\frac{\Delta p}{\mu*L_{Dia}}$
Outflow Rate	$\dot{V}$	$K_0*w*\frac{(p*\varepsilon)^{x+1}*\beta^y}{\tau^{z+1}}*\frac{\Delta p*A_{Dia}}{\mu*L_{Dia}}$
Conductivity	S_{ohm}	$\frac{1}{\rho_{ohm}}*w*\frac{(p*\varepsilon)^{x+1}*\beta^y}{\tau^{z+1}}*\frac{A_{Dia}}{L_{Dia}}$
Overall Performance	P	$\frac{1}{L_{Dia}*\rho_{ohm}}*\left[\frac{1}{4\beta}+\frac{1}{2\sqrt{\beta}}+\frac{1}{4}\right]*w*\frac{(p*\varepsilon)^x*\beta^y}{\tau^{z+1}}$

2.2.2. Validating the Model by Comparison to CFD

Those aspects of the model concerning flow through the pores (velocity and flow rate calculation), have been validated by conducting OpenFoam®-based CFD calculations. As shown in Figure 4, material samples were analysed by FIB-tomography, then their microstructure was digitalised (top-left, top-middle) [25]-[30] and transferred into a finite volume mesh (top-right).

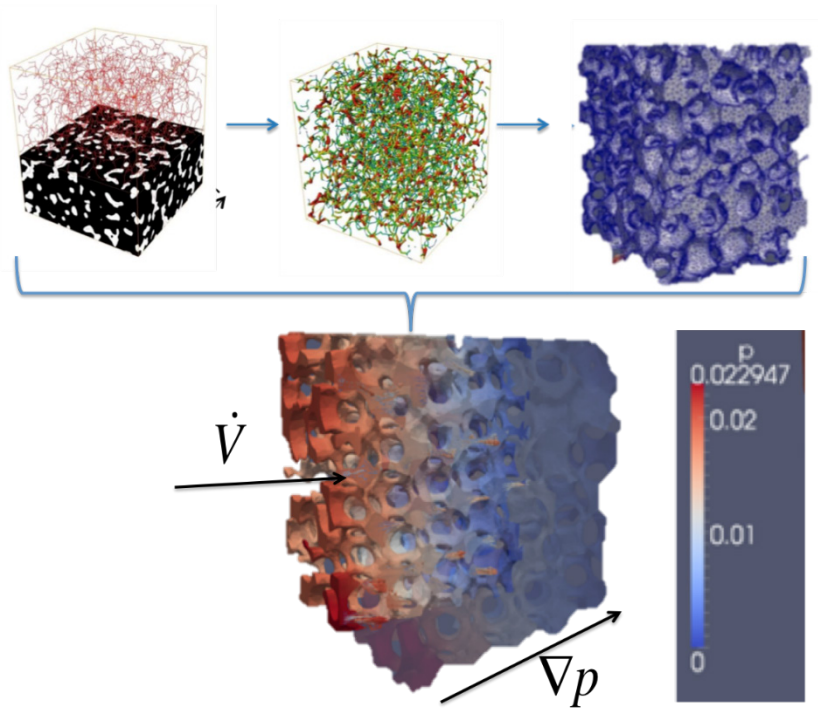

Figure 4: Qualitative example of FIB-tomography data (top-left, top-middle) of ceramic material sample (diameter ca. 10µm, voxel resolution ca. 10-20nm) [25]-[30] and corresponding finite volume mesh (top-right), as well as coloured representation of pressure field within microstructure, based on OpenFoam® simulations with icoFoam solver (bottom).

The simple case of viscid, single phase, creeping flow, driven by a given pressure gradient of ≈0.5bar/mm, was modelled by using the OpenFoam®-based ico Foam solver, converging to a steady state (Figure 4, bottom).

In order to get a reasonable sense of the quality of our model-based permeability predictions the following steps were conducted:

(i) Three different types of material matrices were analyzed, digitalized and evaluated by FIB-tomography according [1], [25]-[30];

(ii) The presence of pore-former additive was simulated by adding five different amounts of spherical pores per reconstructed matrix-type;

(iii) The electrolyte flow through those digital material samples was then simulated by OpenFoam® and predicted by our model;

The results of this validation procedure are depicted in Figure 5, where the relative change of outflow-rate, compared to a reference material sample is printed out against the relative amount of added pore former. Based on these results, it can be shown that deviations between well known and widely validated CFD simulations and our model predictions are lower than 12%. This result is valid within a relatively wide range of microstructure properties and a pressure gradient of ≈0.5bar/mm. It can be seen that the semi-analytical model shows a slight systematic overestimation of flow rate deviations.

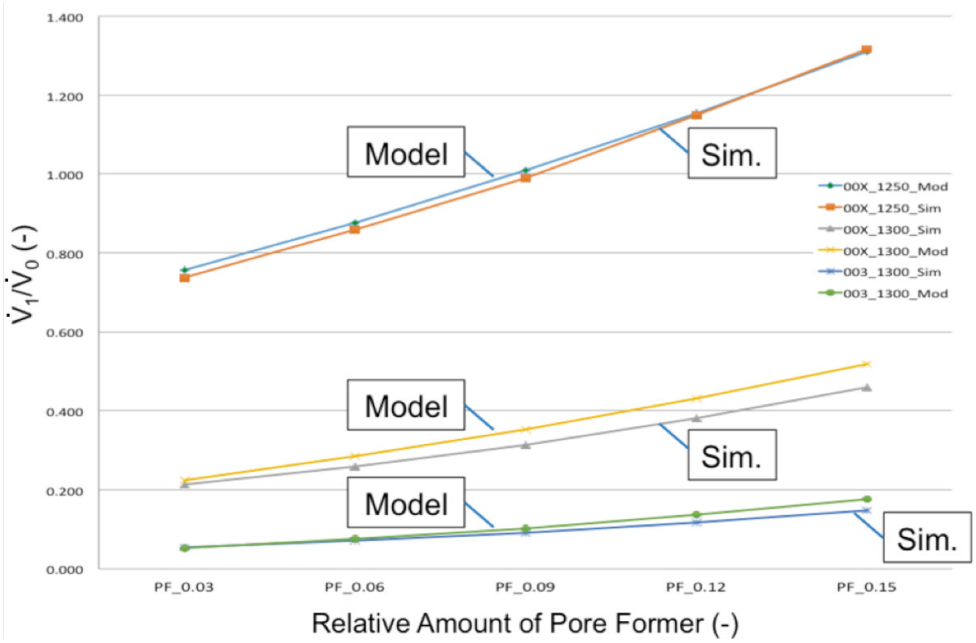

Figure 5: Ratio of outflow rate of current- (index 1) to reference- (index 0) design option against five different relative amounts of pore former (3%, 6%, 9%, 12% and 15%). Three pairs of material matrices inspected by OpenFoam®-based CFD simulation ("Sim.") and our semi-analytical model ("Model") are shown in direct comparison. Largest found deviations are <12%.

2.2.3. Comparing Design Options by Introduction of Dimensionless Design Factors

In order to evaluate the impact of design parameter modifications on the process variables to be improved, a dimensionless approach is imperative. To achieve this, dimensionless design factors $F_{i,j}$ are introduced. They relate any design parameter $\Psi_{i,j}$ of type i and design option j to its adapted counterpart within a new design option j+1, according Eqn. 11.

$$F_{i,j} = \frac{\Psi_{i,j+1}}{\Psi_{i,j}} \tag{11}$$

While Table 1 (right column) denotes all design factors to their respective design parameters, Table 3 shows how a change of design factors impacts the relation of essential process variables $\Phi_{i,j}$, according to Eqn. 12.

$$\frac{\Phi_{i,j+1}}{\Phi_{i,j}} = f\left(F_{i,j}\right) \tag{12}$$

Table 3: Ratios of process variables $\Phi_{i,j+1}/\ \Phi_{i,j}$ of type i, belonging to consecutive design options j+1 and j as well as their context to the dimensionless design factors $F_{i,j}$ according to the semi-analytical model.

Process Variable to be improved	**Ratio between design Options $\Phi_{i,j+1}/\ \Phi_{i,j}$**	**Context to Design Factors $\Phi_{i,j+1}/\ \Phi_{i,j} = f(F_{i,j})$**
Maximum Outflow Velocity	$v_{\max,j+1} / v_{\max,j}$	$\frac{e^x * f^{y-1}}{g^{z+1}} * \frac{c}{b*d} * \left(\frac{1+2*\sqrt{f\beta_j}+f\beta_j}{1+2*\sqrt{\beta_j}+\beta_j}\right)$
Outflow Rate	$\dot{V}_{j+1} / \dot{V}_j$	$\frac{e^{x+1} f^y}{g^{z+1}} * \frac{c*a}{b*d}$
Diaphragm Conductivity	$S_{ohm,j+1} / S_{ohm,j}$	$\frac{e^{x+1} f^y}{g^{z+1}} * \frac{a}{b} * \frac{1}{h}$
Over all Performance	$\left(\frac{S_{ohm} * v_{\max}}{\dot{V}}\right)_{j+1} / \left(\frac{S_{ohm} * v_{\max}}{\dot{V}}\right)_j$	$\left(\frac{e^x * f^{y-1}}{g^{z+1}} * \frac{1}{b} * \frac{1}{h}\right) * \left(\frac{1+2*\sqrt{f\beta_j}+f\beta_j}{1+2*\sqrt{\beta_j}+\beta_j}\right)$

2.2.4. Measures to Improve Individual Improvement Criteria

The relations shown in Table 3 already contain generalized information on how to improve individual process variables, according to the *improvement criteria* defined in chapter 2.1.2. Table 4 provides an overview of the measures, derived from Table 3.

Table 4: Overview of measures to independently modify process variables such that their respective improvement criterion is matched more closely, by design parameter increase ("+") or decrease ("-"). Non-dependencies are marked by "x".

Parameter Type	**Design Parameter**	**Velocity Criterion:** $v_{\max} \to \max.$	**Flow-Rate Criterion:** $\dot{V} \to \min.$	**Conductivity Criterion:** $S_{ohm} \to \max.$
Ceramic Macro-Structure	Length of Diaphragm	-	+	-
	Cross Section of Diaphragm	X	+	+
Ceramic Micro-Structure	Pore Constrictivity	-	-	+
	Pore Tortuosity	-	+	-
	Porosity	+	-	+
Process	Pressure Difference	+	-	x
Electrolyte	Dynamic Viscosity	-	+	X
	Intrinsic Resistivity	X	x	-

2.2.5. From Individual Parameters to System Approach: The Dependency Diagram

Table 4 clearly demonstrates that, adapting one single design parameter to improve performance with respect to one individual improvement criterion might cause problems with respect to other criteria. Thus, a system-based approach is needed, which considers all design parameter-criteria-interactions as well as respective degrees of proportionality. A first step in this context is the depiction of a dependency diagram, as seen in Figure 6.

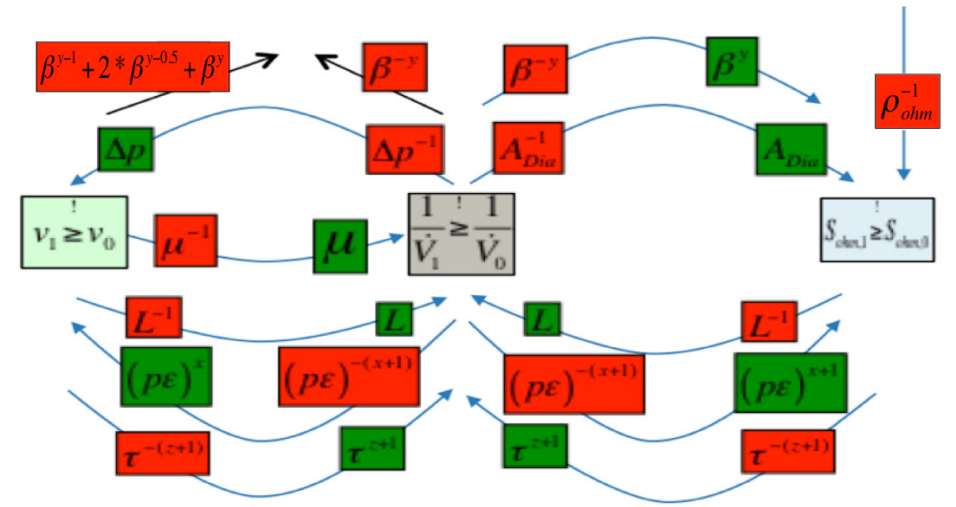

Figure 6: Dependency diagram depicting all *design parameter*-criteria-interactions. Red coloration means that the respective criterion will "suffer" according the denoted proportionality, as the design parameter is increased. Green coloration means that the respective criterion will "benefit" according the denoted proportionality, as the design parameter is increased. Note that the coefficients are x=1.15, y=0.37 and z=4.39 [1], that indices "1" and "0" are used for design options j+1 and j respectively and that p is a constant proportionality factor relating the porosity to the cross-sectional area of an individual pore, according chapter 2.2.1.

2.2.6. Introducing the Switching Factors α, β and Ω

A mere overview of all design-parameter-criteria-interactions does not suffice to allow for a controlled "switching of focus" between the improvement criteria from one design option to the next. Thus, the switching factors α, β and Ω have been introduced. They are ratios between design options and their focus in regard to selected improvement criteria.

Switching Factor α

According to Eqn.13, α relates the development of the velocity criterion to the development of the flow rate criterion as design option j shifts to design option j+1. If α>1 then the focus obviously shifts from flow rate criterion to velocity criterion. This means that, if design option j+1 is chosen, starting from option j and α is >1, then the relative increase of outflow velocity will outweigh the relative decrease of outflow rate.

$$\alpha = \frac{v_{\max,j+1} * \dot{V}_{j+1}}{v_{\max,j} * \dot{V}_j} \tag{13}$$

Eqn.14 shows how α relates to the individual design factors $F_{i,j}$ which connect the design parameters $\Psi_{i,j}$ and $\Psi_{i,j+1}$.

$$\alpha = \frac{e^{2x+1} f^{2y-1}}{g^{2z+2}} * \frac{c^2 * a}{b^2 * d^2} * \left(\frac{1 + 2 * \sqrt{f\beta_j} + f\beta_j}{1 + 2 * \sqrt{\beta_j} + \beta_j} \right) \tag{14}$$

Switching Factor β

According to Eqn.15, β relates the development of the *flow rate criterion* to the development of the *conductivity criterion* as design option j shifts to design option j+1. If β>1 then the focus obviously shifts from *conductivity criterion* to *flow rate criterion*. This means that, if design option j+1 is chosen, starting from option j and β is >1, then the relative decrease of outflow rate will outweigh the relative increase of conductivity.

$$\beta = \frac{\dot{V}_j * S_{ohm,j}}{\dot{V}_{j+1} * S_{ohm,j+1}} \tag{15}$$

Eqn.16 shows how β relates to the individual design factors $F_{i,j}$ which connect the design parameters $\Psi_{i,j}$ and $\Psi_{i,j+1}$.

$$\beta = \frac{g^{2z+2}}{e^{2x+2} * f^{2y}} * \frac{b^2 * d}{a^2 * c} * h \tag{16}$$

Switching Factor or Performance Factor Ω

The *switching factor* Ω is hereby also called the *performance factor*. This is because, according to Eqn.17, Ω relates all *improvement criteria* as design option j shifts to design option j+1. If Ω>1 then the relative change in process variables improving the overall performance, outweighs the relative change in process variables decreasing overall performance.

$$\Omega = \frac{S_{ohm,j+1} * v_{\max,j+1} * \dot{V}_j}{\dot{V}_{j+1} * S_{ohm,j} * v_{\max,j}} \tag{17}$$

Eqn.18 shows how Ω relates to the individual *design factors* $F_{i,j}$ which connects the design parameters $\Psi_{i,j}$ and $\Psi_{i,j+1}$.

$$\Omega = \frac{e^x * f^{y-1}}{g^{z+1}} * \frac{1}{b} * \left(\frac{1 + 2 * \sqrt{f\beta_j} + f\beta_j}{1 + 2 * \sqrt{\beta_j} + \beta_j} \right) * \frac{1}{h} \tag{18}$$

These definitions and dependencies can be re-formulated such that the development of the process variables to be improved Φ_i, can be shown in relation to a certain set of chosen switching factors as seen in Eqn.19.

$$\frac{\Phi_{i,j+1}}{\Phi_{i,j}} = f(\alpha, \beta, \Omega) \tag{19}$$

The necessary equations are summarized in Table 5. Note that, in order for this scheme to make physical sense, all *switching factors* must be larger than zero.

Table 5: Overview of process variable ratios between design options j+1 and j and their context to the dimensionless switching factors α, β and Ω according to Eqn.13 to Eqn.19. All switching factors must be larger than zero.

Process Variable to be improved	**Ratio between Design Options $\Phi_{i,j+1}/\Phi_{i,j}$**	**Context to Switching Factors $\Phi_{i,j}+1/\Phi_{i,j} = f(\alpha,\beta,\Omega)$**
Maximum Outflow Velocity	$v_{\max,j+1} / v_{\max,j}$	$\alpha * \sqrt[3]{\frac{\beta*\Omega}{\alpha}}$
Outflow Rate	$\dot{V}_{j+1} / \dot{V}_j$	$\sqrt[3]{\frac{\alpha}{\beta*\Omega}}$
Diaphragm Conductivity	$S_{ohm,j+1} / S_{ohm,j}$	$\frac{1}{\beta} * \sqrt[3]{\frac{\beta*\Omega}{\alpha}}$
Over all Performance	$\left(\frac{S_{ohm} * v_{\max}}{\dot{V}}\right)_{j+1} / \left(\frac{S_{ohm} * v_{\max}}{\dot{V}}\right)_j$	Ω

3. RESULTS

On the basis of the model assumptions, definitions and according derivations within chapter 2, some concrete measures of how to improve diaphragm performance can now be presented in chapter 3.1. Furthermore a method to find design options to simultaneously improve all process variables in terms of *improvement criteria* is shown in chapter 3.2. The improvement space concept introduced there, can also be used to shift the focus between various *improvement criteria* in a very controlled way.

3.1. Increasing the Overall Performance by Adjustment of Ω

The performance factor Ω relates all process variables in terms of *improvement criteria*. Thus an increase of Ω can be counted as an increase of the overall performance of the diaphragm.

Note that an increase of Ω does not necessarily mean that design option j+1 is better with respect to all individual *improvement criteria*, but rather that relative improvements outweigh the setbacks. Having that in mind, an inspection of Eqn.18 provides valuable insights on how to improve the overall performance of a diaphragm by adjusting the related *design factors*. Thus several essential design guidelines can be extracted. They are summarized in Table 6.

Table 6: Overview of impact of design parameter changes on performance factor and related design guidelines. Favorable design parameter increase is denoted as "+", favorable design parameter decrease is marked as "-". Non-dependencies are marked with "x".

Parameter Type	Design Parameter	Performance Factor Ω	Design Guideline
Ceramic Macro-Structure	Length of Diaphragm	-	Aim for short diaphragm and short pores
	Cross Section of Diaphragm	x	Choose small cross section if durability is limiting and large cross-section if accuracy is limiting
Ceramic Micro-Structure	Pore Constrictivity	-	Aim for pores with well-defined bottlenecks to achieve low constrictivity
	Pore Tortuosity	-	Aim for straight pores to achieve low tortuosity
	Porosity	+	Prefer material with high open flow porosity
Process	Pressure Difference	x	Choose high pressure difference if accuracy is limiting and low pressure difference if durability is limiting
Electrolyte	Dynamic Viscosity	x	Choose high electrolyte viscosity if durability is limiting and low viscosity if accuracy is limiting
	Intrinsic Resistivity	-	Choose electrolyte with low intrinsic resistivity

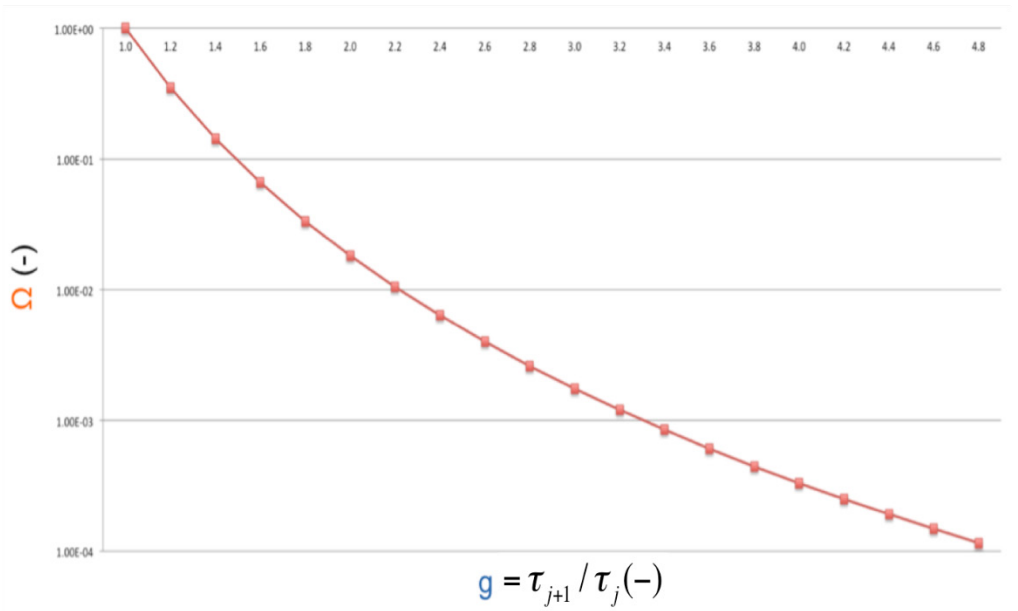

Figure 7: Dimensionless performance factor Ω against dimensionless tortuosity-related design factor g. Increasing tortuosity means lower overall diaphragm performance.

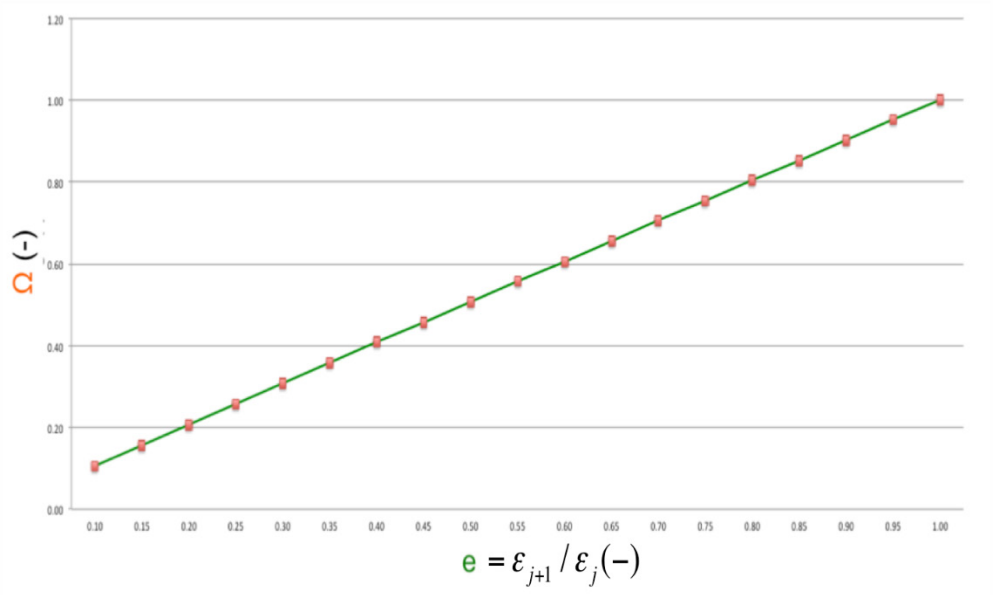

Figure 8: Dimensionless performance factor Ω against dimensionless porosity-related design factor e. increasing porosity means higher overall diaphragm performance.

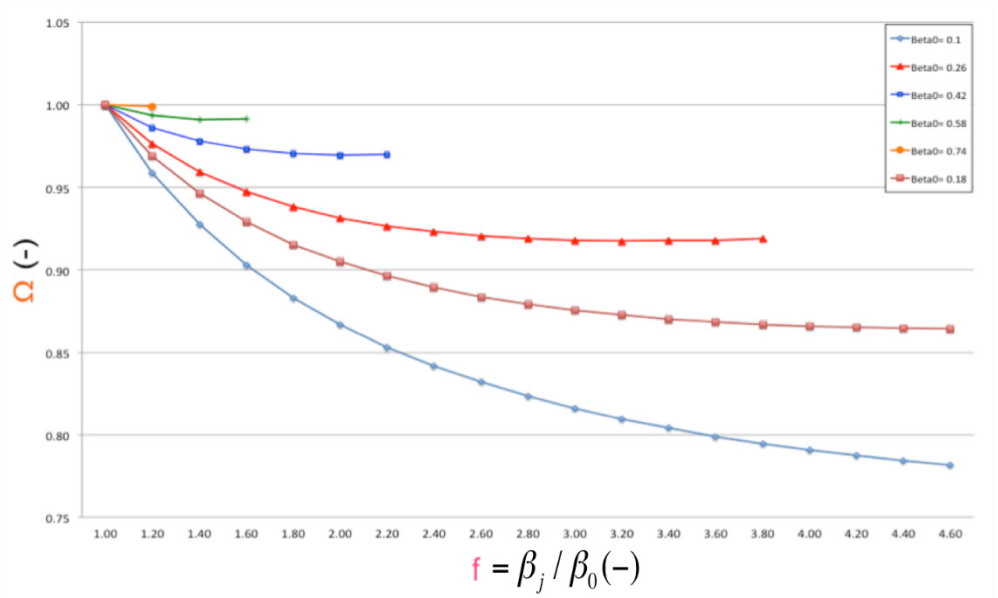

Figure 9: Dimensionless performance factor Ω against dimensionless constrictivity-related design factor f. Graphs are parameterized by reference sample constrictivity β_0. Increasing constrictivity means lower overall diaphragm performance. If reference sample constrictivity is low, the effect is more pronounced.

3.2. Introducing the Improvement Space Concept

Practical application has shown that it is not always enough to have design guidelines to increase overall performance as defined by the relation of process variables and *improvement criteria*. Quite frequently material samples exist, which excel in one or two out of three improvement criteria already, but lack behind expectations regarding the others. Thus, a tool is required to shift the focus between *improvement criteria*, while simultaneously increasing or at least keeping overall performance of the medium. This requirement has led to the introduction of the *improvement space concept*.

The improvement space features three dimensions: the switching factors α, β and Ω. Thus movement within that space always means a change from reference design option j (α=1, β=1, Ω=1) to any advanced design option j+1 ($0<\alpha<\infty$, $0<\beta<\infty$, $\Omega\geq1$). More specifically, movement in each one of the three directions means the following:

Direction α>1

New design option j+1 will feature higher outflow velocity (good) but also higher outflow rate (bad).

Direction β>1

New design option j+1 will feature lower outflow rate (good) but also lower conductivity (bad).

Direction Ω>1

New design option j+1 will feature higher overall performance (good) and thus more options to perform better in regard to anyone of the improvement criteria.

Let Ω be constant and ≥1, then the improvement space turns into an improvement plane, which is illustrated in Figure 10, along with typical regional features.

Figure 10: Conceptual illustration of the improvement plane for constant Ω≥1.

Assuming the concrete example, of diaphragm length reduction of 13% (b=0.87), Ω becomes 1.15. Now a range of design options emerges which allow for a certain freedom of movement within α- (shifting between velocity and flow rate) and β- (shifting between flow rate and conductivity) direction, while diaphragm performance with respect to every single improvement criterion can still be achieved. Figure 11 illustrates design options with higher conductivity (bottom, right, green), with lower flow rate (bottom, left, green), with higher outflow velocity (top, right, green) and design options which perform better with respect to all three criteria (top, left, green). Note that the green triangle within the top, left subplot of Figure 11 represents the intersection of the three individual improvement zones. It is found by intersecting the three critical functions where $\Phi_{i,j+1}/\Phi_{i,j}=1$. These critical borderlines can be derived from Table 5 and are stated in Eqn.20, Eqn.21 and Eqn.22.

For $S_{ohmj+1}/S_{ohm,j}=1$:

$$\beta * \Omega * \alpha^2 = 1 \tag{20}$$

For $v_{max,j+1}/v_{max,j}=1$:

$$\beta * \Omega * \alpha^{-1} = 1 \tag{21}$$

For $V_{j+1}/V_j=1$:

$$\beta * \Omega^{-1/2} * \alpha^{1/2} = 1 \tag{22}$$

Also, note that the corners of the improvement triangle represent design options where one particular improvement criterion is emphasized, while the others remain unchanged, as compared to the reference case. Thus, the top-left corner (intersection between conductivity-borderline and velocity-borderline) corresponds to a minimization of flow rate, the top-right corner (intersection between conductivity-borderline and flow rate borderline) corresponds to a maximization of flow velocity and the bottom-center corner (intersection between velocity-borderline and flow rate borderline) corresponds to a maximization of conductivity.

The full improvement space becomes accessible, when $\Omega \geq 1$ can be varied as well. As the performance factor Ω increases, the overall diaphragm improvement triangle within the α-β plane gets larger and larger, as seen in Figure 12.

Since the improvement space is a completely non-dimensional concept, it is universally applicable as long as the model assumptions (chapter 2) hold. The generalized procedure of sensibly applying the improvement space concept can be summarized as follows:

(i) Choose reference sample j, analyze its design parameters (according Table 1) and process variables (maximum outflow velocity, conductivity and outflow rate) in relation to any target values.

(ii) Choose any one of the design-guidelines proposed in Table 6, to obtain a performance factor $\Omega>1$.

(iii) Calculate the new performance factor for the relation between new design option j+1 and reference case j, according Eqn.18.

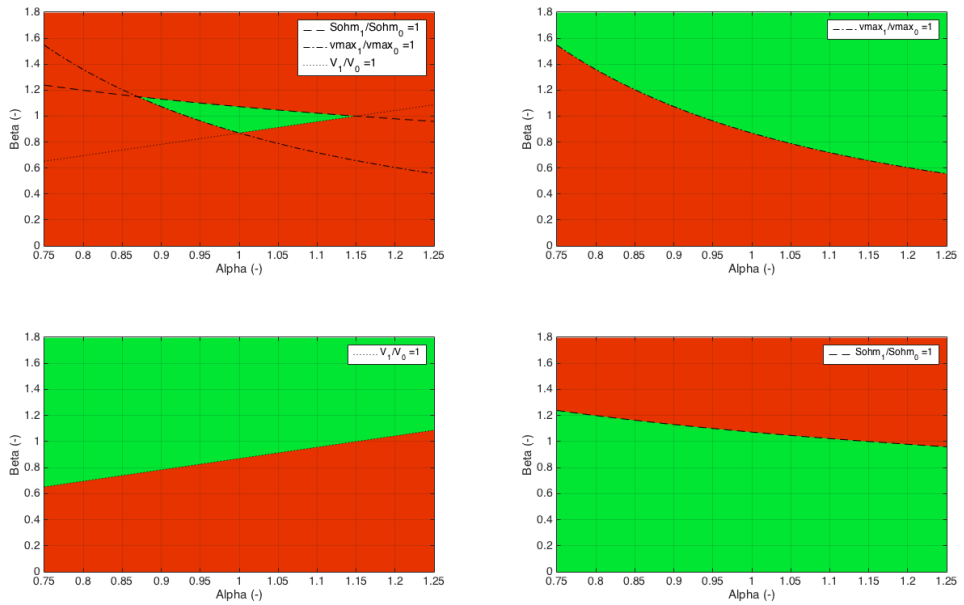

Figure 11: Illustration of improvement zones (green) for conductivity criterion (bottom, right), flow rate criterion (bottom, left), velocity criterion (top, right) and the overall diaphragm improvement triangle (top left) for Ω=1.15. Red zones symbolize design options where at least one of the three (velocity, flow rate, conductivity) improvement criteria gets worse.

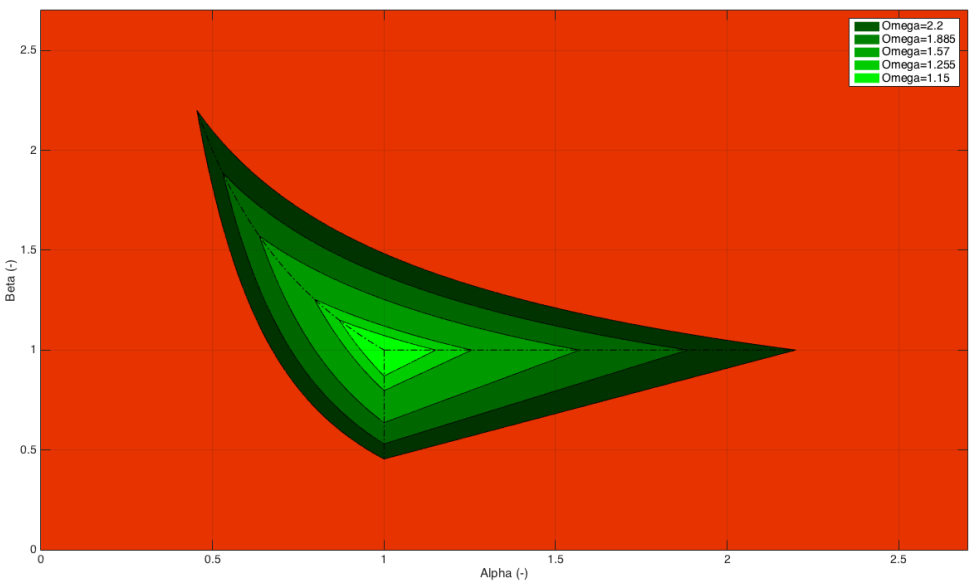

Figure 12: Diaphragm improvement triangle (green tones) where each improvement criterion gets "better", as it gets larger with increasing performance factor Ω. Red zone symbolizes design options where at least one of the three (velocity, flow rate, conductivity) improvement criteria gets "worse".

(iv) Draw the critical borderlines according Eqn.20 to Eqn.22 in α-β space to obtain an improvement triangle, as seen in Figure 12, with Ω being the parameter.

(v) Choose suitable α or β values to obtain any desired process variables of design option j+1 in relation to reference case j.

(vi) Use α, β and Ω values, as well as process variables of reference design option j to verify process variables of new design option j+1, according Table 5.

(vii) Use relations from Table 3, as well as chosen restrictions and design parameters of reference case j to calculate design factors and corresponding design parameters of new design option j+1.

4. CONCLUSION

In total, a method was presented which allows the controlled modification of a ceramic diaphragm, applied as liquid junction in pH-probes. This multi-parameter improvement method is designed to increase, shift and adapt the diaphragm's performance in regard to three distinct improvement criteria: (i) the maximization of outflow velocity through the pores, (ii) the minimization of electrolyte outflow rate and (iii) the maximization of electric conductivity.

In this context, a semi-analytical model was developed to relate diaphragm design parameters as well as their dimensionless design factors to process variables and their respective improvement criteria. The model was validated by comparison to well-established OpenFoam®-based CFD simulations, conducted within digitally reconstructed and modified material sample meshes. The dependencies found within the semi-analytic model, were then evaluated and used to introduce the switching factors α and β, as well as the performance factor Ω. The latter was found to represent one way to define and thus increase overall diaphragm performance.

On this basis it is hereby proposed that a new, improved diaphragm design option should feature high porosity, low constrictivity and low tortuosity, thus it should yield many, straight pores with defined bottlenecks. Furthermore the sample should be as short as possible and the electrolyte should feature low intrinsic resistivity. Design parameters such as diaphragm cross section, electrolyte viscosity or internal probe over-pressure do not generally lead to an increase or decrease of the overall performance, but can rather be used to balance out two improvement criteria at a time.

REFERENCES

[1] L. Holzer, O. Stenzel, O. Pecho, T. Ott, G. Boiger, M. Gorbar, Y. de Hazan, D. Penner, I. Schneider, R. Cervera, P. Gasser, Fundamental relationships between 3D pore topology, electrolyte conduction and flow properties: Towards knowledge-based design of ceramic diaphragms for sensor applications, Materials & Design, Volume 99, 5 June 2016, Pages 314-327

[2] M. Gorbar, D. Penner, Y. de Hazan, L. Holzer, G. Boiger, R.J. Cervera, Extrusion of YSZ diaphragms with controlled porosity used as liquid junction in pH electrodes; 14th International Conference of European Ceramic Society, 21 – 25 June 2015; Toledo, Spain, conference proceedings.

[3] M. Gorbar, D. Penner, Y. de Hazan, L. Holzer, G. Boiger, R.J. Cervera, Controlled Porous Microstructure and its Effect on Transport Properties within YSZ Diaphragms of pH Electrodes; Venue: 6th International Congress on Ceramics, 21 – 25 August 2016; Dresden Germany, conference proceedings;

[4] R.G. Bates, A.K. Vijh, Determination of pH: theory and practice, J. Electrochem. Soc.120 (1973) 263C

[5] H. Suzuki, H. Shiroishi, S. Sasaki, I. Karube, Microfabricated liquid junction Ag/AgCl reference electrode and its application to a one-chip potentiometric sensor, Anal.Chem. 71 (1999) 5069–5075

[6] J.W. Severinghaus, Design of capillary pH electrode incorporating an open liquid junction and reference electrode in a single unit, Scand. J. Clin. Lab. Invest. 17(1965) 614–616

[7] J.J. Pedrotti, L. Angnes, I.G.R. Gutz, Miniaturized reference electrodes with microporous polymer junctions, Electroanalysis 8 (1996) 673–675

[8] D.P. Brezinski, Kinetic, static and stirring errors of liquid junction reference electrodes, Analyst 108 (1983) 425–442

[9] J.A. Illingworth, A common source of error in pH measurements, Biochem. J. 195(1981) 259–262

[10] Mettler-Toledo AG, Urdorf, Guide-lines of pH-measurement: Theory and practical application, http://www.mt.com/dam/MTPRO/PDF/GUIDE/pH_Theory_Guide_de_30105455_Oct13.pdf, 2013 (accessed October 5, 2013).

[11] C.F. Berg, Re-examining Archie's law: conductance description by tortuosity and constriction, Phys. Rev. E 86 (2012) 046314, http://dx.doi.org/10.1103/PhysRevE.86.046314.

[12] O. Stenzel, M. Neumann O. Pecho, V. Schmidt, L. Holzer, Predicting effective conductivities based on geometric microstructure characteristics, AICHE J. in press

[13] M.B. Clennell, Tortuosity: a guide through the maze, in: M.A. Lovell, P.K. Harvey (Eds.),Dev. Petrophysics, Geol. Soc. Spec. Publ. No. 122 1997, pp. 299–344.

[14] C.F. Berg, Permeability description by characteristic length, tortuosity, constriction and porosity, Transp. Porous Media 103 (2014) 381–400

[15] G. Gaiselmann, M. Neumann, V. Schmidt, O. Pecho, T. Hocker, L. Holzer, Quantitative relationships between microstructure and effective transport properties based on virtual materials testing, AICHE J. 60 (2014) 1983–1999

[16] E.E. Petersen, Diffusion in a pore of varying cross section, AICHE J. 4 (1958) 343–345.

[17] L. Holzer, D. Wiedenmann, B. Münch, L. Keller, M. Prestat, P. Gasser, et al., The influence of constrictivity on the effective transport properties of porous layers in electrolysis and fuel cells, J. Mater. Sci. 48 (2013) 2934–2952

[18] J. Van Brakel, P.M. Heertjes, Analysis of diffusion in macro-porous media in terms of a porosity, a tortuosity and a constrictivity factor, Int. J. Heat Mass Transf. 1093–1103(1974).

[19] O. Pecho, O. Stenzel, B. Iwanschitz, P. Gasser,M. Neumann, V. Schmidt, et al., 3D microstructure effects in Ni-YSZ Anodes: Prediction of effective transport properties and optimization of redox stability, Materials 8 (2015) 5554–5585

[20] A. Costa, Permeability-porosity relationship: A re-examination of the Kozeny-Carman equation based on a fractal pore-space geometry assumption, Geophys. Res. Lett. 33 (2006), L02318

[21] G.E. Archie, The electrical resistivity log as an aid in determining some reservoir characteristics, Trans. AIME 146–154 (1942).

[22] R.B. Bird,W.E. Steward, E.N. Lightfood, Transport Phenomena, second ed. JohnWiley& Sons, New York, 2007.

[23] M.I.S. Azzam, F.A.L. Dullien, Flow in tubes with periodic step changes in diameter: a numerical solution, Chem. Eng. Sci. 32 (1977) 1445–1455.

[24] S. Sisavath, X. Jing, R. W. Zimmerman, Creeping flow through a pipe of varying radius, Physics of Fluid, Vol.13, No.10, (2001=, 10.1063/1.1399289

[25] B. Münch, L. Holzer, Contradicting geometrical concepts in pore size analysis attained with electron microscopy and mercury intrusion, J. Am. Ceram. Soc. 91(2008) 4059–4067.

[26] L. Holzer, F. Indutnyi, P. Gasser, B. Münch,M. Wegmann, Three-dimensional analysis of porous BaTiO3 ceramics using FIB nano-tomography, J. Microsc. 216 (2004) 84–95.

[27] L. Holzer,M. Cantoni, Review of FIB-Tomography, in: I. Utke, S. Moshkalev, P. Russell (Eds.), Nanofabrication Using Focused Ion and Electron Beams: Principles and Applications, Oxford University Press, New York 2011, pp. 410–435.

[28] M. Cantoni, L. Holzer, Advances in 3D focused ion beam tomography, MRS Bull. 39(2014) 354–360

[29] B. Münch, L. Holzer, Contradicting geometrical concepts in pore size analysis attained with electron microscopy and mercury intrusion, J. Am. Ceram. Soc. 91(2008) 4059–4067

[30] K. Thulasiraman,M.N.S. Swamy, Graphs, Theory and Algorithms, JohnWiley & Sons, New York, 1992.